Supporting Information for

Axially Coordinated Co-N_4 Sites for Nitrobenzene Electroreduction

Meilan Pan[a], Junjian Li[a], Xue Zhang[a], Subiao Liu[c], Jia Wei Chew[b], and Bingjun Pan[a]*

[a] College of Environment, Zhejiang University of Technology, Hangzhou, Zhejiang 310014, China

[b] School of Chemical and Biomedical Engineering, Singapore Membrane Technology Centre, Nanyang Environmental and Water Research Institute, Nanyang Technological University, Singapore 637141, Singapore

[c] School of Minerals Processing and Bioengineering, Central South University, Changsha, Hunan 410083, China

The specific activity was calculated by normalizing the removal amounts of pollutants with the active surface areas (SSA (Equation 1)):

$$Specific\ activity = \frac{(C_0 - C) \times V}{SSA \times m} \quad (1)$$

where C is the effluent concentration of pollutants, C_0 is the influent concentration of pollutants, SSA is the specific surface area (**Table S2**), T is the reaction volume and m is the mass of catalysts. The TOF was calculated by normalizing the removal amounts of pollutants with the Co atomic contents:

$$\text{TOF} = \frac{(C_0 - C) \times V}{n \times T} \quad (2)$$

where R is the removal efficiency and n is the amount of Co atoms measured by ICP-OES analysis in **Table S1**.

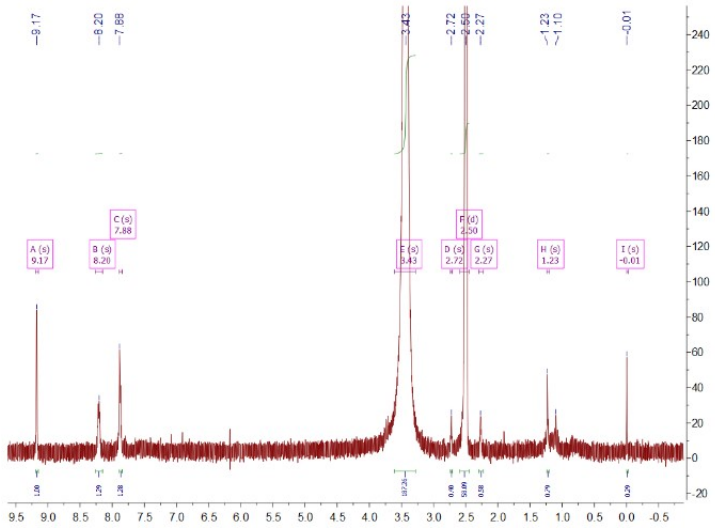

Fig. S1. NMR spectra of CoTFP.

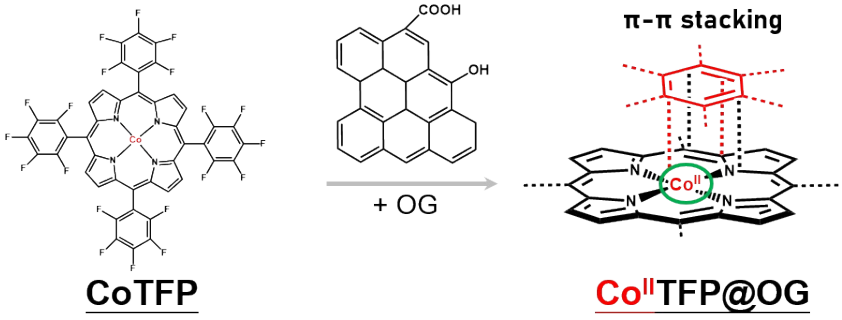

Fig. S2. Scheme illustrates CoTFP interacting with OG through the π-π stacking.

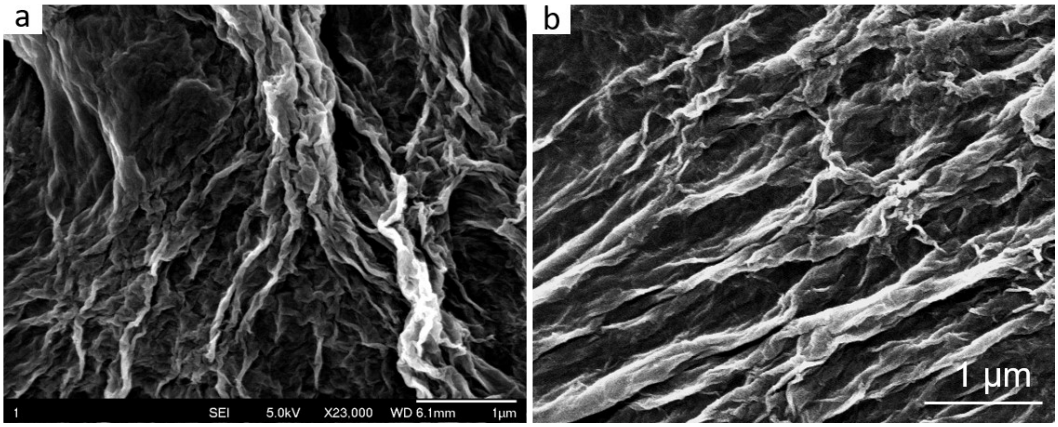

Fig. S3. SEM images of Co^{I}TFP@NG.

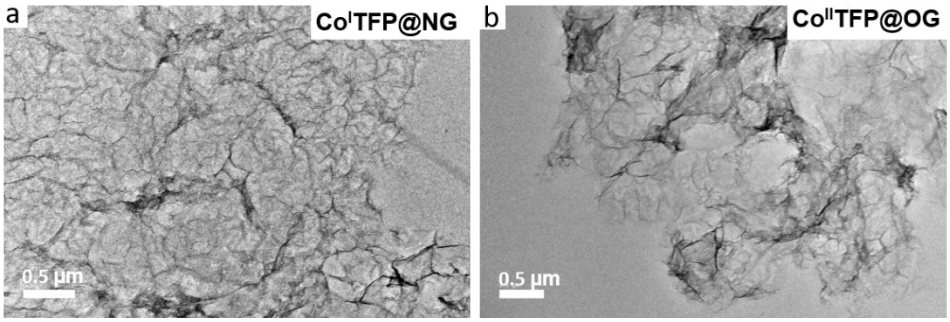

Fig. S4. TEM images of Co^{I}TFP@NG (a) and Co^{II}TFP@OG (b).

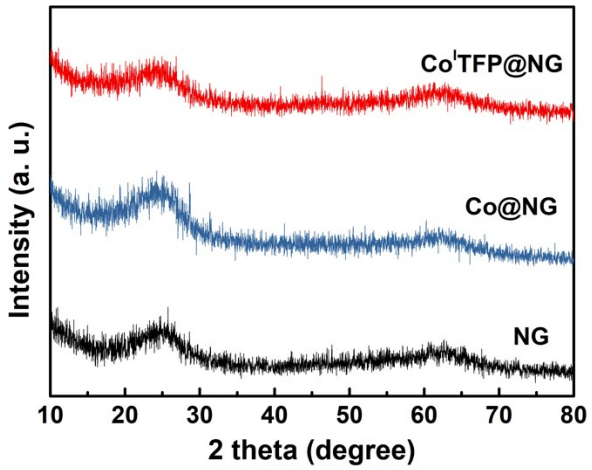

Fig. S5. XRD patterns of NG, Co@NG, and Co^{I}TFP@NG.

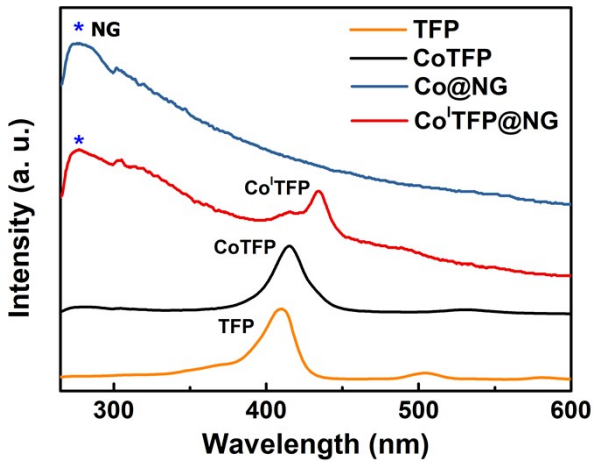

Fig. S6. UV-vis spectra of Co^{I}TFP@NG, Co@NG, TFP, and CoTFP.

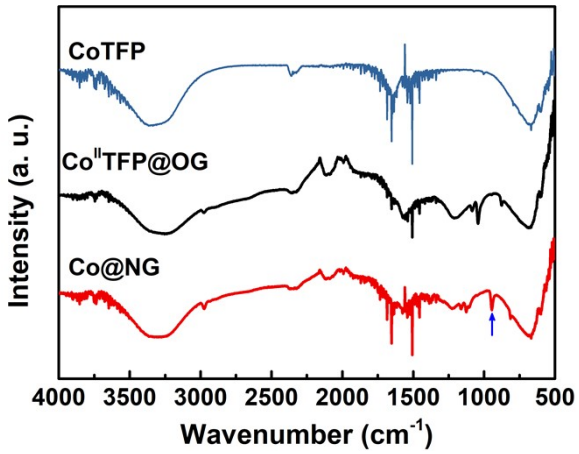

Fig. S7. FTIR spectra of CoTFP, Co@NG, and Co^{II}TFP@OG.

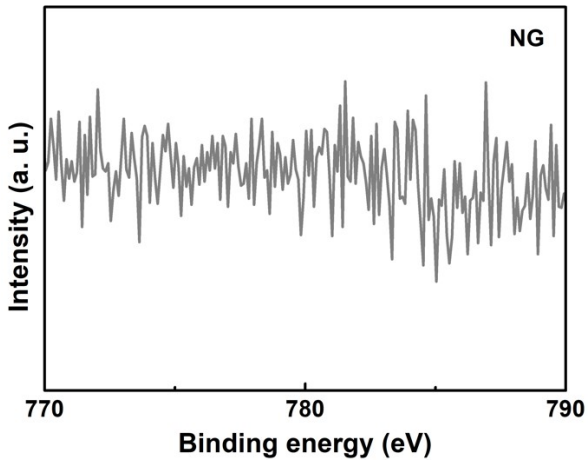

Fig. S8. Co 2p of XPS analysis of NG.

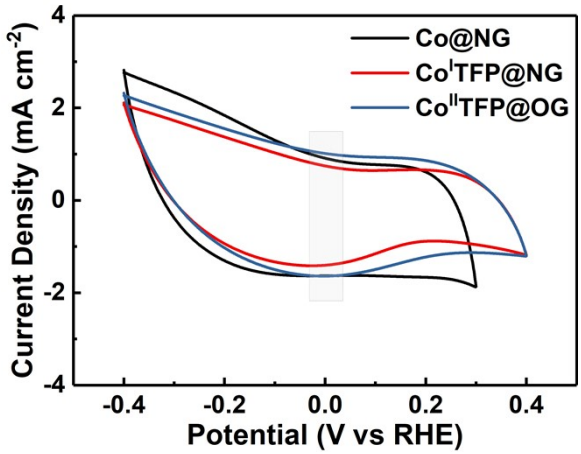

Fig. S9. CV curves of Co@NG, Co^{I}TFP@NG, and Co^{II}TFP@OG in 0.1 M Na_2SO_4.

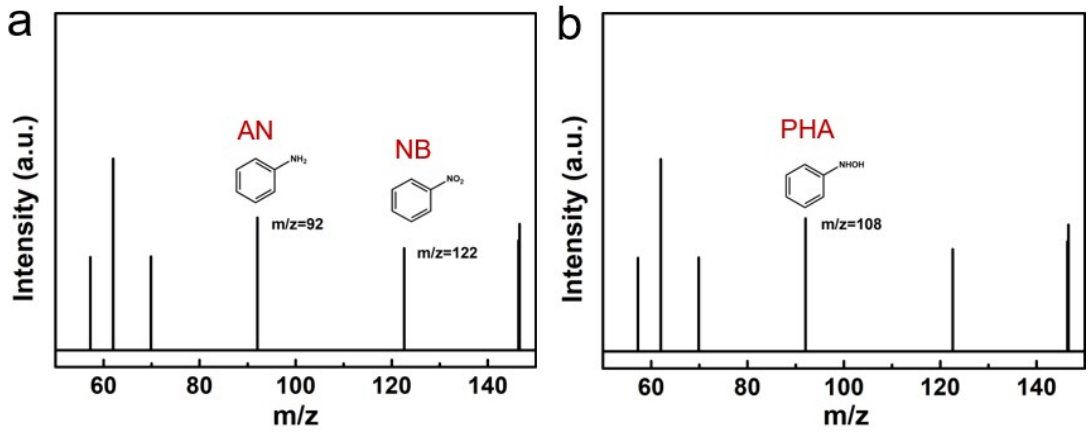

Fig. S10. MS identification of AN, PHA, and NB by HPLC/MS/MS

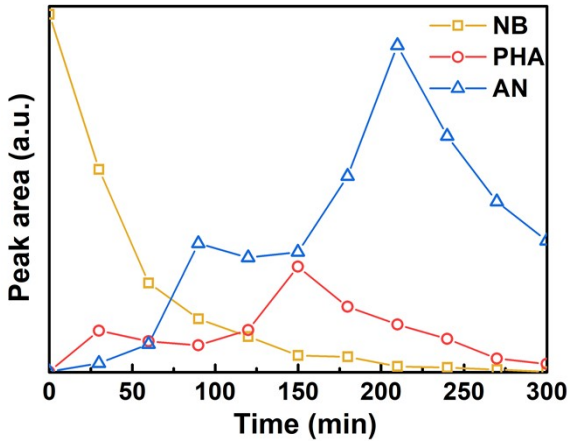

Fig. S11 Evolution of reduction products and NB during electrochemical degradation by Co^{I}TFP@NG.

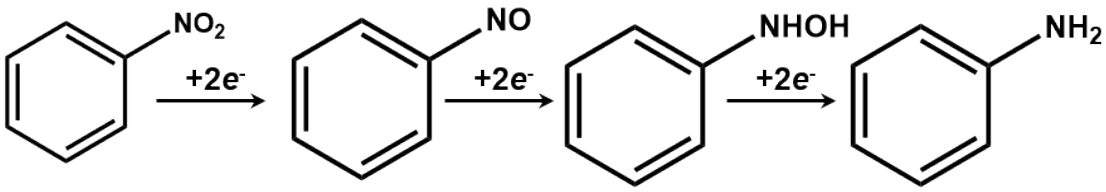

Scheme S1. The electron transport route for reductive electron on NB.

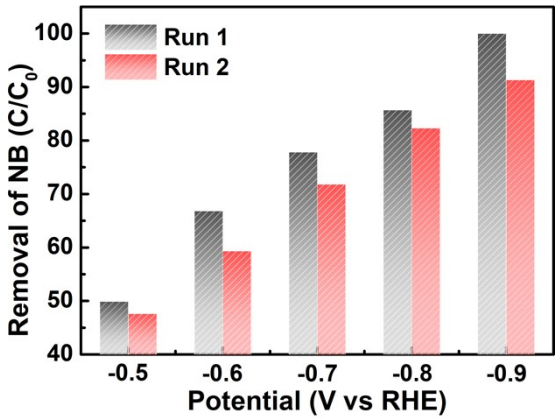

Fig. S12 Stability of Co^{I}TFP@NG.

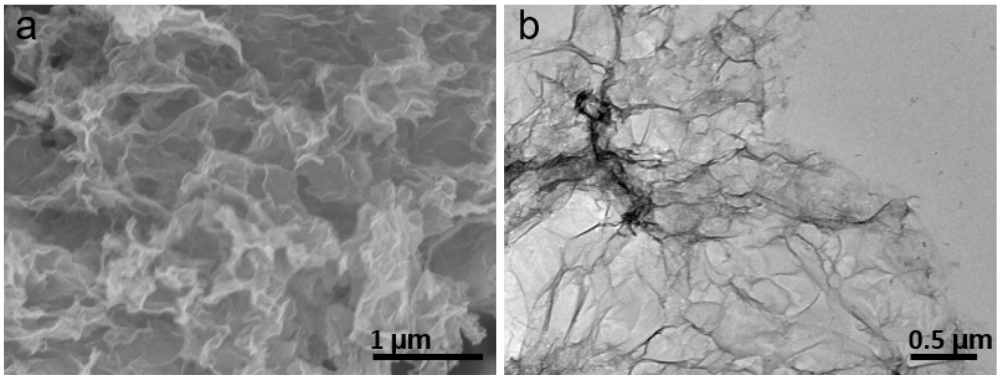

Fig. S13. SEM (a) and TEM (b) image of Co^{I}TFP@NG after reaction.

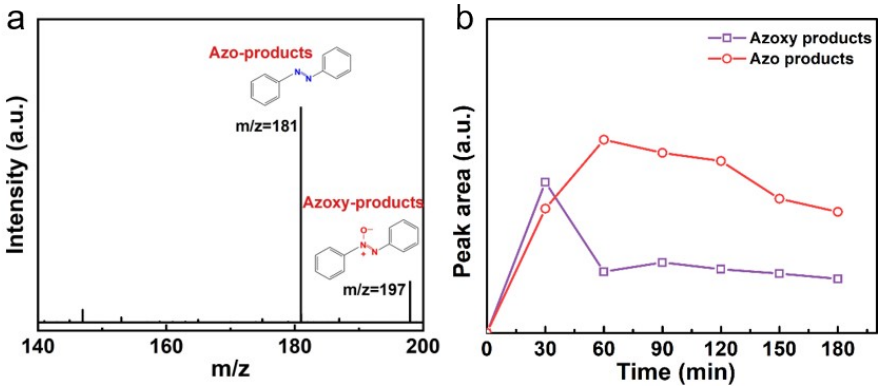

Fig. S14. MS identification of azo-products and azoxy-products by HPLC/MS/MS (a) and their evolution with reaction time.

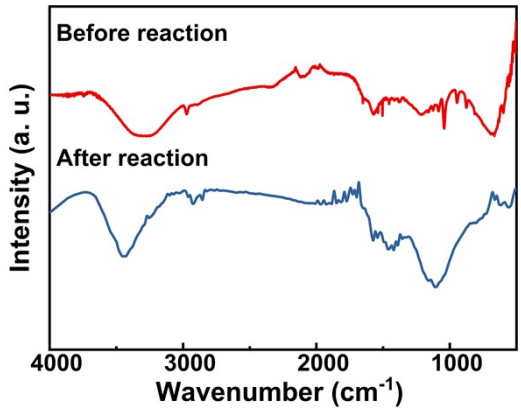

Fig. S15. FTIR spectra of Co^{I}TFP@NG before and after reaction

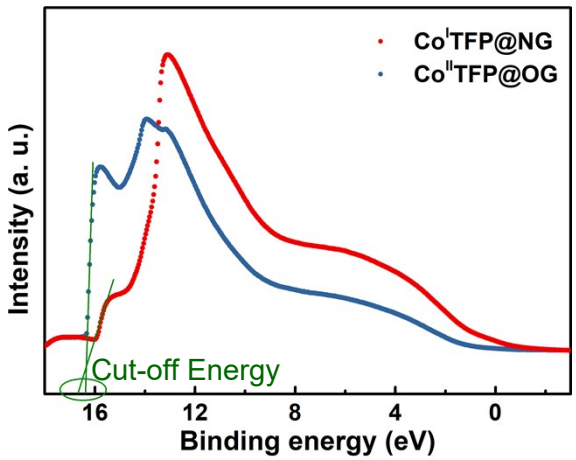

Fig. S16. UPS plots of Co^{I}TFP@NG and Co^{II}TFP@OG.

Table S1. I_D/I_G values and atomic contents of OG, NG, TFP@NG, Co@NG, Co^{I}TFP@NG and Co^{II}TFP@OG based on the measurements of elemental analyzer combined with measurements of inductively coupled plasma spectrometer.

	Co at%	N at%	C at%	H at%	O at%	I_D/I_G
OG	0	0	69.90	13.50	16.60	1.01
NG	0	2.99	43.89	40.20	12.92	1.17
TFP@NG	0	2.51	37.90	47.73	11.86	1.11
Co@NG	0.28	2.64	39.90	44.78	12.40	1.06
Co^{II}TFP@OG	0.14	0.58	48.27	35.41	15.60	1.02
Co^{I}TFP@NG	0.08	0.63	48.24	34.08	16.96	1.05

Table S2. Specific surface area of NG, Co@NG, TFP@NG, Co^{II}TFP@OG, and Co^{I}TFP@NG

Samples	SSA (m^2 g^{-1})	Pore Volume (cm^3 g^{-1})	Pore size (nm)
Co@NG	330.8	0.28	3.2
Co^{II}TFP@OG	314.8	0.22	2.9
Co^{I}TFP@NG	318.2	0.25	3.1

Table S3. Simulated EIS resistance of Co^{I}TFP@NG, Co^{II}TFP@OG, and Co@NG in the NB solution.

	$\mathbf{R_s}$	$\mathbf{R_{ct}}$	$\mathbf{W_{mt}}$
Co^{I}TFP@NG	6.76	12.0	6.58×10^{-2}
Co^{II}TFP@OG	5.28	83.2	2.0×10^{-2}
Co@NG	7.32	105.9	4.88×10^{-3}